

Performance Prediction of a Cavitating Rim Driven Tunnel Thruster

Spyros A. Kinnas¹, Shu-Hao Chang¹, Lei He¹, Jahn Terje Johannessen²

¹Ocean Engineering Group, Department of Civil, Architectural and Environmental Engineering
The University of Texas at Austin, Austin, Texas, USA

²R&T Department, Rolls-Royce Marine AS, N-6065 Ulsteinvik, Norway

ABSTRACT

This paper presents an approach which combines a vortex-lattice method (MPUF-3A) with a RANS solver (FLUENT) for the unsteady flow analysis to predict the effective wake of rim driven tunnel thrusters. The time-averaged propeller body force distributions, which represent the thruster effect, are taken as source terms in the momentum equations of FLUENT. After the effective wake is achieved by the coupling method, a boundary element method (PROPCAV) will use this effective wake as an inflow to calculate the performance of tunnel thrusters. The effect of the viscosity on the effective wake is evaluated through MPUF-3A/FLUENT coupling. The results of the coupling method MPUF-3A/FLUENT are validated with those calculated from PROPCAV and those measured in the experiments. The results of MPUF-3A/FLUENT and PROPCAV show that the coupling method can predict reasonable forces. In addition, the MPUF-3A/FLUENT coupling method and PROPCAV appear to predict the extent of cavitation reasonably well.

Keywords

Vortex-Lattice Method (VLM), Reynolds-Averaged Navier Stokes (RANS) solver, Effective wake, Rim driven tunnel thruster, Boundary Element Method (BEM)

1 INTRODUCTION

In recent decades, the increasing demand for high-speed ocean vehicles in commercial or navy applications has primarily driven the design of propulsion systems. For marine propulsors, complex propulsion configurations are becoming more and more common in order to reach the requirements of high efficiency performance, safety, comfort and cost effective maintenance. As a result, a tunnel thruster which is based on a compact permanent magnet solution (inside a sealed rim of the propeller rotor), excited by an electro-magnetic field, has become an appropriate alternative in the contemporary design. Similar to many other marine propellers, cavitation also affects the performance of a tunnel thrust propulsion system. However, the elimination of the need for vertical shaft and gearing, which connect the electric motor and the propeller blades as in a conventional design, can decrease a turbulent inflow generated by the gear housing stay, brackets or other flow obstructions to the propeller

and lower the noise and vibration levels. Compared with the conventional design, another important feature is no clearance between the propeller blades and the tunnel wall. Therefore, the tip leakage vortex can be avoided and associated flow problems can be minimized.

In order to assess the performance of a cavitating rim propeller, the first important step is to predict the effective inflow wake appropriately. In the previous study, Choi and Kinnas (2003) used an Euler solver and a Vortex-Lattice coupled method to predict an unsteady effective wake. Kinnas et al. (2006) applied a Vortex-Lattice method with an Euler solver and a Reynolds-Averaged Navier Stokes solver for the unsteady flow analysis and performance of various types of podded propellers.

The next step is to predict the cavities on the propeller blades. Recently, Kinnas et al. (1998) applied a panel method which can predict partial and/or super cavity by iterative method inside of a square tunnel. Later, Bal et al. (2001, 2003) extended this method for the analysis of 2-D and 3-D cavitating hydrofoils inside of a numerical wave tank with a free surface. In addition, Choi and Kinnas (1998, 1999) predicted the propeller performance inside of a tunnel by coupling of a lifting surface method and a boundary element method. In their methods, however, the unsteady cavitating propeller and the tunnel problem are solved separately, and the effect of one on another is accounted for in an iterative manner.

In this paper, PROPCAV, a boundary element method, is used to predict cavitating performance of a tunnel thruster with the complete tunnel wall effect. A vortex-lattice method (MPUF-3A) is coupled with FLUENT (a commercial RANS solver) in order to evaluate the effective wake to be used in PROPCAV. In this study, only the sheet cavitation on the propeller blades is addressed. The cavitating flow inside of a tunnel thruster is analyzed by using a low order potential based boundary element method which is the same as that used by Lee and Kinnas (2005) and Sun and Kinnas (2008). The integral equations for the tunnel thruster problem satisfy the Green's third identity, and are solved directly by distributing constant sources and dipoles over the blades, hub and tunnel surfaces, and constant dipoles on the wake

surfaces. The cavitation on the blade and wake surfaces is determined by applying the dynamic and kinematic boundary conditions on the cavity surface.

A prototype version of a rim driven tunnel thruster (RDTT), designed by Rolls-Royce Marine, will be studied by using MPUF-3A/FLUENT coupling method to obtain the effective wake first, and then the steady and unsteady cavitating performance of the propeller will be evaluated by MPUF-3A and PROPCAV. Results obtained from both methods will be compared with those from measurements.

2 METHODOLOGY

2.1 Effective wake prediction

Effective wake is defined as the total velocity less the induced velocity by the propeller.

$$\vec{q}_e(\vec{x}, t) = \vec{q}_t(\vec{x}, t) - \vec{q}_p(\vec{x}, t) \quad (1)$$

Where the subscripts, e, t , and p denote effective, total, and propeller induced velocity, respectively.

Prediction of effective wake is crucial for predicting propeller performance by using a potential solver. In this research, an iterative process is introduced between VLM solver (MPUF-3A) and RANS solver (FLUENT) to evaluate the effective wake. At the initial step, a uniform inflow wake is inputted into VLM solver. The propeller loading and pressure distributions on blade surface are computed. The propeller loading is converted into body forces which will present the propeller effect in the calculation of RANS solver. The body forces can be obtained by integrating the pressure difference, Δp , on the blade surface A_c . The dimensionless body forces are given as follows:

$$\vec{f} = \left(\frac{4R^3}{vJ_s^2} \right) \vec{F}_p, \quad \vec{F}_p = \frac{\Delta p A_c \vec{n}}{\rho n^2 D^4} \quad (2)$$

Where R and D are the radius and diameter of the blade, J_s is an advance ratio, and v is the cell volume. F_p is the dimensionless pressure force from MPUF-3A. ρ and n are the water density and rotating speed. \vec{n} is the normal vector.

The RANS solver then solves for the fluid domain with these body force distributions. Once the computation of FLUENT is finished, the effective wake can be obtained by subtracting the propeller induced velocity from the total velocity. The VLM solver continues to use the updated wake as an inflow in the calculation. The iterations are performed between VLM and RANS solvers until the converged solution is obtained. The iterative process is shown in Figure 1.

2.2 Vortex-Lattice method (MPUF-3A)

A Vortex-Lattice method named MPUF-3A is used to simulate the cavitating or wetted propeller potential flow subject to an effective inflow. In VLM, the blade loading and blade or cavity thickness are represented by the discrete line vortices and line sources. The line vortices

and line sources are placed on the mean camber surface and on the transition wake. The unknown strength of the singularities is determined by applying the kinematic boundary condition and dynamic boundary condition. The kinematic boundary condition requires that the normal component of the total velocity on the mean camber surface equals zero. The dynamic boundary condition requires that the pressure on the cavity surface equals the vapor pressure. In this method, the effect of hub and tunnel is included by using simplified image model, in which each vortex and source segments are imaged with respect to hub and tunnel radius. Figure 2 shows the geometry of the tunnel thruster used in MPUF-3A calculation.

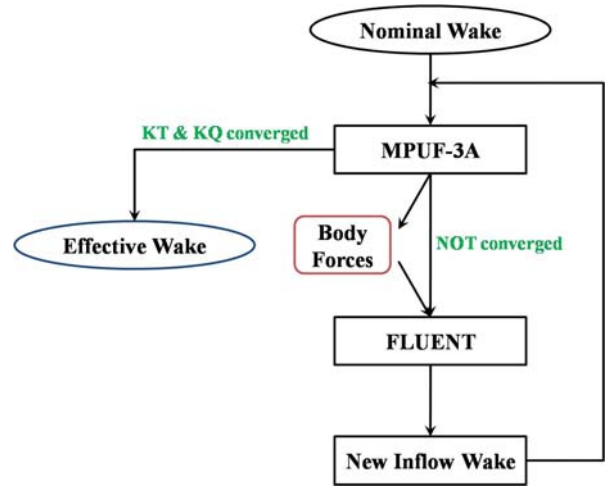


Figure 1: Flow chart of the iterative method between MPUF-3A and FLUENT.

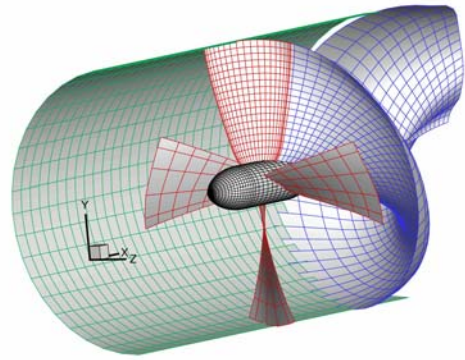


Figure 2: Geometry of RDTT tunnel thruster (the key blade uses 20x18 grids and other blades use coarser grids). View from upstream.

2.3 RANS solver (FLUENT)

In this research, a commercial RANS solver FLUENT is used to simulate the viscous flow around the propeller inside of a tunnel. In FLUENT, the governing equations are solved for the conservation of mass and momentum by using finite volume method. The rotating propeller effect is included in the form of time-averaged body force

momentum sources obtained from MPUF-3A. Figure 3 shows the body force distributions used in FLUENT at $J_s = 0.941$.

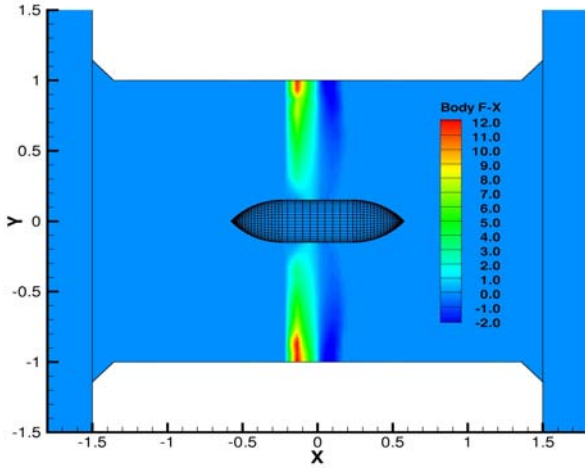


Figure 3: Axial body force distribution in FLUENT at $J_s = 0.941$, $RPM = 925$. The values are non-dimensionalized by using equation (2).

The standard $k-\varepsilon$ turbulence model is used to solve RANS equations. $Re = JsnD^2 / 2\nu = 1.02 \times 10^6$ at $J_s = 0.941$ and $RPM = 925$. Pressure-velocity coupling is achieved by using SIMPLE algorithm. The boundary condition for the tunnel surface is set as a no-slip wall with Standard Wall Functions applied. The steady 3-D simulations were performed on the non-structured grids generated from GAMBIT with boundary layers attached on the tunnel wall surface so that $y^+ < 350$. In order to include the propeller effect, the momentum equations are modified by adding the body force terms obtained from MPUF-3A by using User-Defined Functions in FLUENT. The convergence criteria are set so that the residuals are smaller than 5×10^{-6} .

2.4 Boundary Element method (PROPCAV)

Consider a 3D cavitating propeller inside of a tunnel subject to a non-axisymmetric inflow. Assume that the fluid in the tunnel is incompressible and inviscid, and thus the flow around the propeller can be taken as a potential flow. Thus, the total flow velocity relative to the propeller fixed coordinate system can be expressed as follows:

$$\vec{q}_t(x, y, z, t) = \vec{q}_{in}(x, y, z, t) + \nabla\phi(x, y, z, t) \quad (3)$$

Where $\vec{q}_t(x, y, z, t)$ is the total velocity, $\vec{q}_{in}(x, y, z, t)$ is the inflow velocity and $\phi(x, y, z, t)$ is the perturbation potential. The perturbation potential satisfies the Laplace's equation in the fluid domain.

$$\nabla^2\phi(x, y, z, t) = 0 \quad (4)$$

By applying Green's third identity with respect to the perturbation potential ϕ at any time, the following integral equation can be achieved:

$$2\pi\phi(\vec{x}, t) = \iint_{S_B+S_C} \left[\phi_q(\vec{x}, t) \frac{\partial G(p; q)}{\partial n_q} - G(p; q) \frac{\partial \phi_q(\vec{x}, t)}{\partial n_q} \right] ds + \iint_{S_w} \Delta\phi_w(\vec{x}, t) \frac{\partial G(p; q)}{\partial n_q} ds + \iint_{S_r} \phi_q(\vec{x}, t) \frac{\partial G(p; q)}{\partial n_q} ds \quad (5)$$

with the subscript q corresponding to the variable points in the integration; n_q is the unit vector normal to the body surface or to the wake surface, $\Delta\phi_w$ is the potential jump at the trailing edge of blades, and $G(p; q)$ is the Green's function. In the case of an unbounded three-dimensional fluid domain, $G(p; q) = 1/R(p; q)$, with $R(p; q)$ being the distance between points p and q . In addition, the kinematic boundary condition is that only a tangential velocity exists on the body surface, as follows:

$$\frac{\partial \phi}{\partial n} = -\nabla\phi \cdot \vec{n} = -\vec{q}_{in} \cdot \vec{n} \quad (6)$$

The inflow and outflow boundary conditions of the tunnel are as follows:

$$\vec{q}_{in} \cdot \vec{n} + \frac{\partial \phi}{\partial n} = \vec{q}_{in} \cdot \vec{n} \quad \text{or} \quad \frac{\partial \phi}{\partial n} = 0 \quad (7)$$

Figure 4 shows the representative panel arrangements of the RDTT tunnel thruster used in PROPCAV.

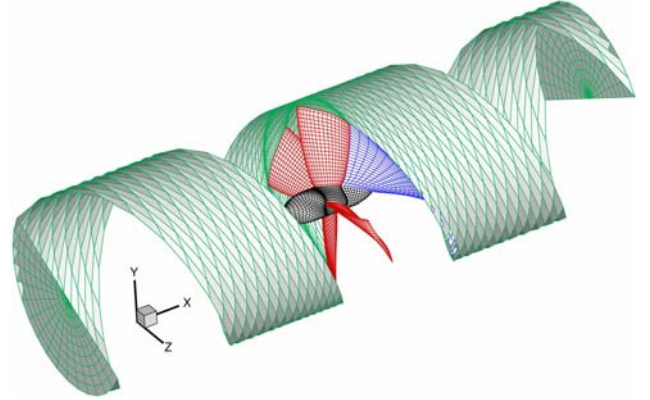


Figure 4: Modeling of RDTT thruster and the tunnel wall in PROPCAV (the panels on the blades are 40x20).

3 NUMERICAL RESULTS

3.1 Effective Wake Prediction

In order to evaluate the appropriate effective wake, the entire domain in FLUENT has been build. The size of the domain is $-19.65 \leq X \leq 26.65$, $-12.855 \leq Y \leq 0.0$, $-13.025 \leq Z \leq 22.525$. The domain size is non-dimensionalized by keeping the propeller radius $R = 1.0$ from the original size of the modeling basin (9.26m x 7.11m x 2.571m) and the size of the modeling tunnel thruster ($R = 0.2m$). Figure 5 shows the computation domain in FLUENT. No-slip wall boundary conditions are applied on the surrounding wall and the bottom of the basin. The upper surface of the basin uses symmetric boundary condition. In Figure 6 and

7 the surface grids on the tunnel thruster and a blowup of the tunnel lid are shown respectively. The modeling tunnel thruster used in the experiment is shown in Figure 8.

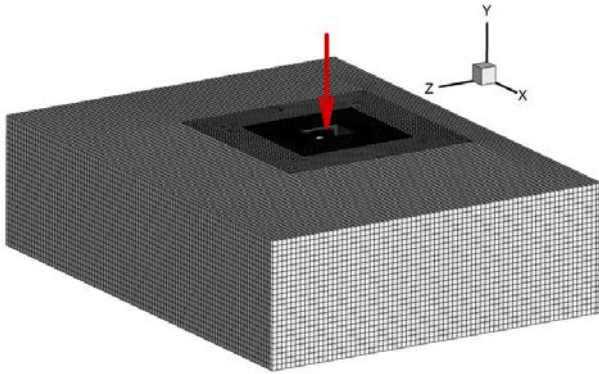


Figure 5: Computational domain in FLUENT. There are three layers of the grids. The inside two layers (darker color) use hexahedral grids and the outside layer uses structured grids. The total number of grids is about 1.4 millions.

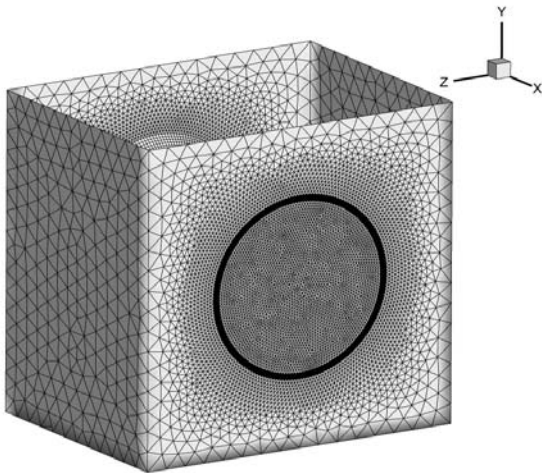


Figure 6: The surface grids on the tunnel thruster. The thruster is at the position where the arrow points at in Figure 5.

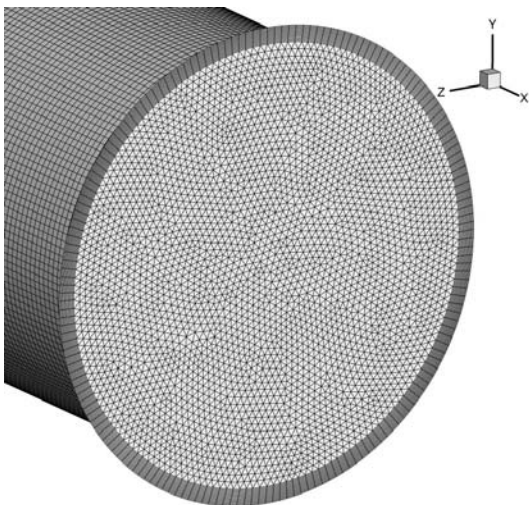


Figure 7: The grids inside of the tunnel are hexahedral with the boundary layer attached on the inner wall.

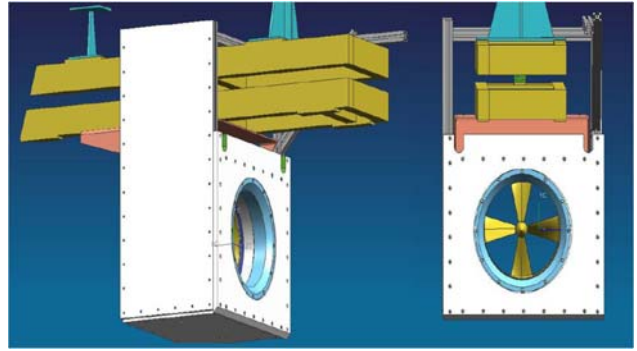


Figure 8: The side view and front view of the modeling tunnel thruster used in the experiment. Compare with the geometry used in FLUENT shown in Figure 6.

Several locations are chosen in FLUENT to evaluate the effective wake as shown in Figure 9. The evaluating surface should be as close to the propeller as possible but cannot intersect with the blade. The iterative process between MPUF-3A and FLUENT will finish when the changing rates of thrust and torque coefficients K_T and K_Q smaller than the convergence criteria 2×10^{-3} . The convergence history of K_T and K_Q calculated from MPUF-3A are shown in Figure 10. Once the iterative process converges, the effective wake can be determined by using equation (1). The axial velocity contours of the effective wake obtained from different locations are shown in Figure 11. The thrust coefficients K_T calculated from MPUF-3A by using the effective wakes determined at different locations is shown in Figure 12. The thrust coefficient obtained by using the effective wake predicted at $X = -0.25$ has a lower value, but the difference is very small as compared with those calculated from other three X locations. The prediction of the performance later in this paper will use the effective wake obtained at surface $X = -0.25$.

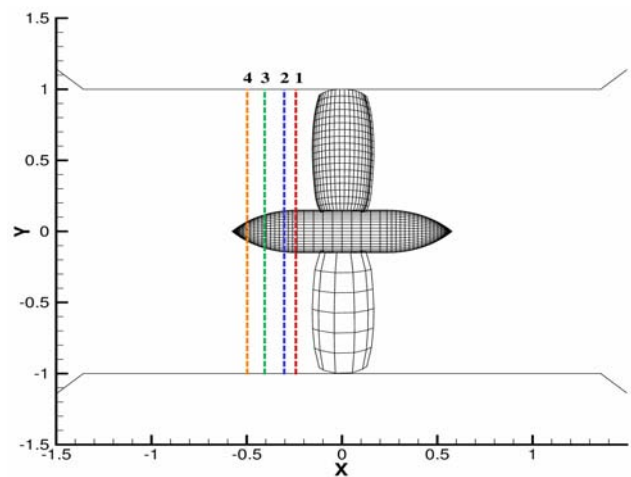


Figure 9: Several evaluating surfaces of the effective wake in FLUENT. The number 1, 2, 3 and 4 denote the surfaces at $X = -0.25, -0.3, -0.4,$ and -0.5 respectively.

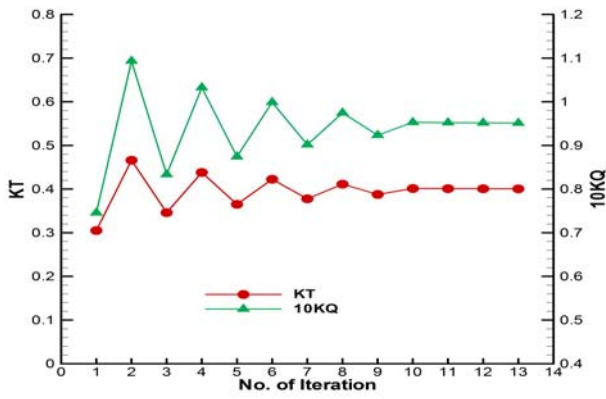


Figure 10: Convergence history of K_T and K_Q from MPUF-3A at $J_s = 0.941$, $RPM = 925$.

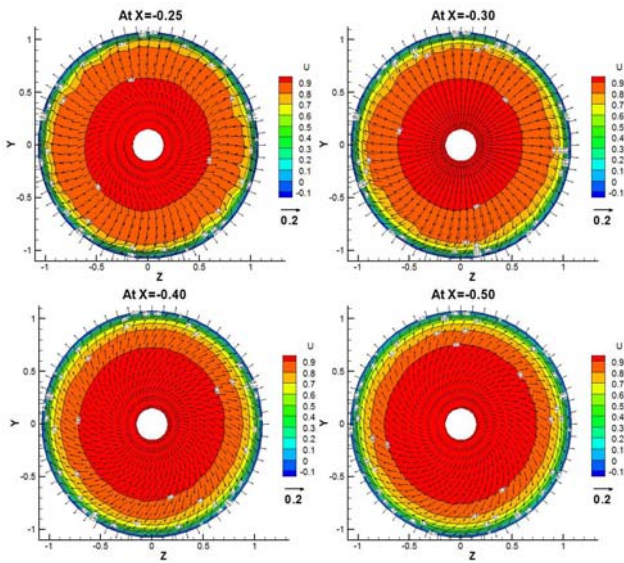


Figure 11: U velocity contours at four axial locations. The propeller plane is at $X = 0$.

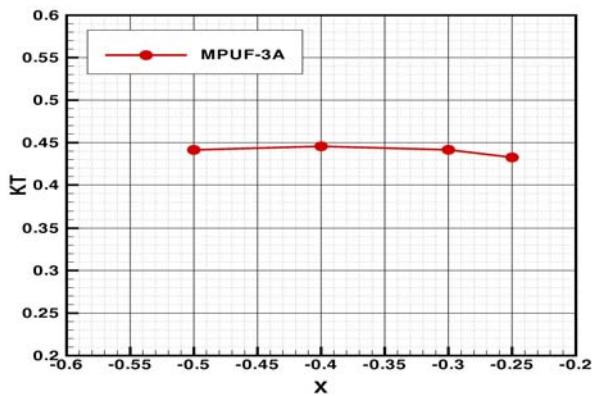


Figure 12: Comparison of K_T by using the effective wakes determined at different locations.

3.2 Performance Prediction by MPUF-3A

After obtaining the effective wake, MPUF-3A then takes this wake as an inflow to calculate the steady and unsteady cavitating flow problems. Cavitating run is

tested at $J_s = 0.941$, $RPM = 925$ and $\sigma_n = 5.31$. Figure 13 shows the unsteady cavitating circulation distributions on the blade. The cavitating pressure distributions at different sections along the span-wise direction are shown in Figure 14 (the blade is at 0°). It should be noticed that the cavitating pressure distributions on the blade are $-C_p = \sigma_n$ on the cavity and $-C_p < \sigma_n$ everywhere else on the blade. The pressures at the blade trailing edge are not closed due to the iterative pressure Kutta condition is not applied in the calculation of MPUF-3A. Figure 15 shows the cavity patterns on the back and face sides of the blade. It is shown that the back cavities start from the leading edge and there are no cavities on the face side.

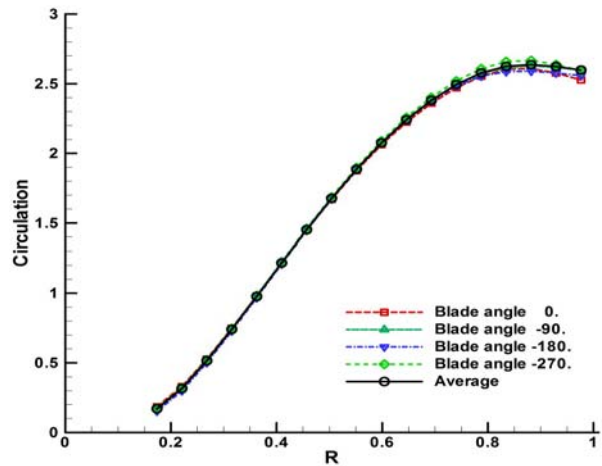


Figure 13: Cavitating circulation distributions on the blade at different angles and the averaged value.

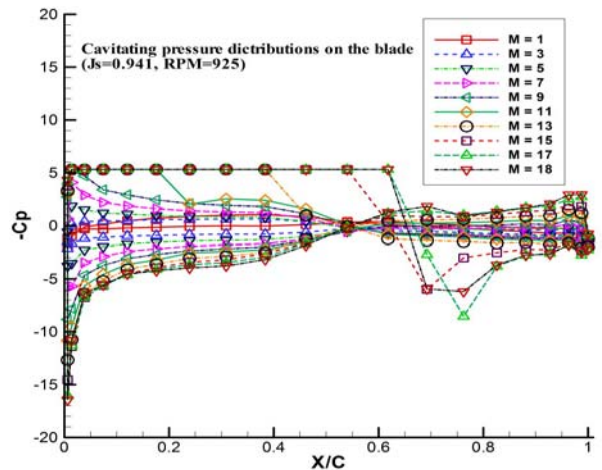


Figure 14: Cavitating pressure distributions on the blade at $J_s = 0.941$, $RPM = 925$ and $\sigma_n = 5.31$ by MPUF-3A (the blade is at 0°).

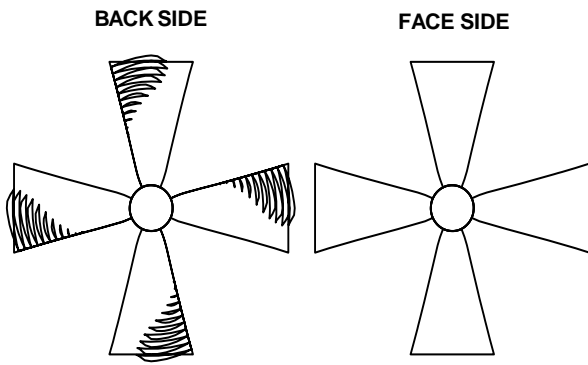


Figure 15: Cavity patterns on the suction side (back) of the thruster blade at $J_s = 0.941$, $RPM = 925$ and $\sigma_n = 5.31$.

3.3 Performance Prediction by PROPCAV

PROPCAV uses the same effective wake obtained from MPUF-3A/FLUENT coupling method as an inflow to calculate the steady cavitating inflow problem. Cavitating run is tested at $J_s = 0.941$, $RPM = 925$ and $\sigma_n = 5.31$. Figure 16 shows steady cavitating circulation distributions on the blade. The predicted cavitating pressure distributions at different sections along the spanwise direction of the blade are shown in Figure 17. Here, the pressures at blade trailing edge between are closed because the iterative pressure Kutta condition has been applied in the calculation of PROPCAV (see Figure 14 and 17). The contour plots of cavitating pressure and the predicted cavity patterns on the back and face sides of the blade are shown in Figure 18 and 19. There are no cavities on the face side.

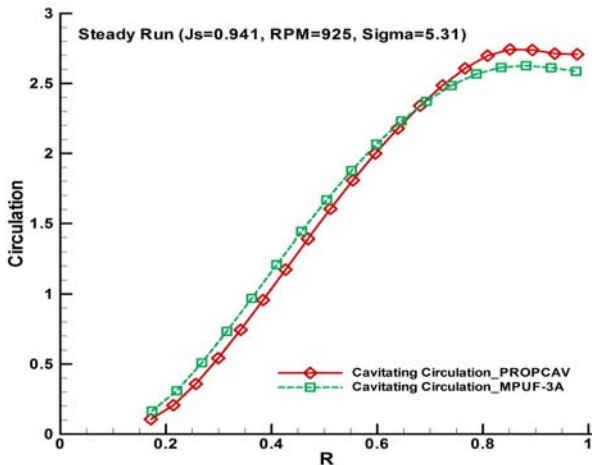


Figure 16: Steady cavitating circulation distributions on the blade from PROPCAV and compared with the results from MPUF-3A.

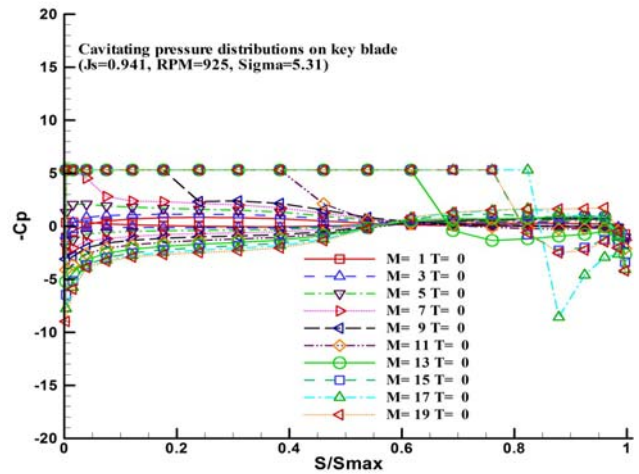


Figure 17: Cavitating pressure distributions on the blade at $J_s = 0.941$, $RPM = 925$ and $\sigma_n = 5.31$ by PROPCAV.

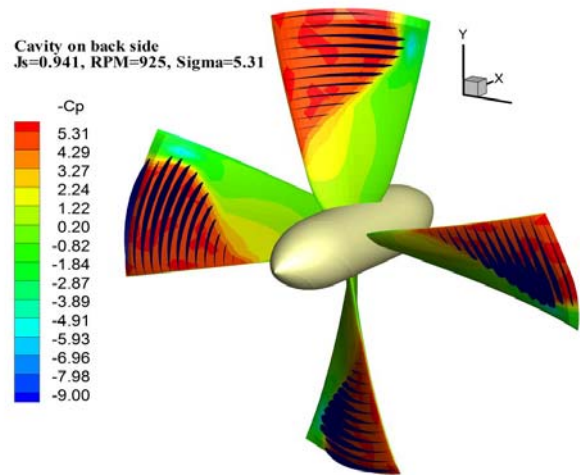


Figure 18: Contour plots of predicted cavitating pressures and cavity patterns on suction (back) side of the blade at $J_s = 0.941$, $RPM = 925$ and $\sigma_n = 5.31$; viewed from upstream.

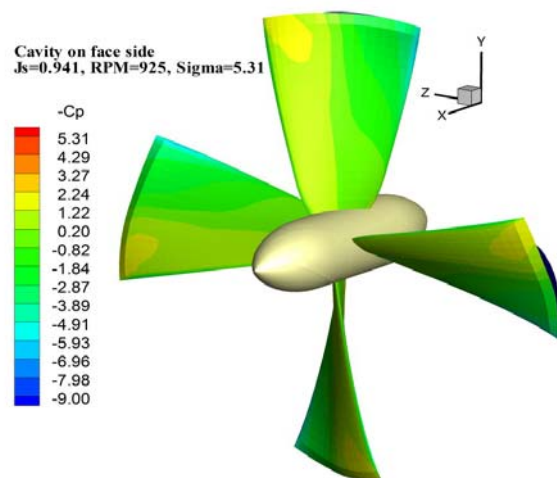


Figure 19: Contour plots of predicted cavitating pressures and cavity patterns on pressure (face) side of the blade at $J_s = 0.941$, $RPM = 925$ and $\sigma_n = 5.31$; viewed from downstream.

3.4 Comparison with Experimental Measurements

The steady cavity patterns predicted by PROPCAV and MPUF-3A are shown in Figure 20. The experimental observations are shown in Figure 21. PROPCAV predicts more cavities than MPUF-3A; therefore, the circulation calculated by PROPCAV is higher than that by MPUF-3A near the blade tip (see Figure 16). The thrust coefficients calculated from PROPCAV and MPUF-3A are also compared with those from the experimental data. The comparison of thrust coefficients is shown in Table 1. Thrusts versus different rotating speed are shown in Figure 22. The relation between the thrust coefficient K_T and the thrust is as follows:

$$Thrust = \rho n^2 D^4 \times K_T \quad (8)$$

Where ρ , n and D are the water density and rotating speed (RPS) and diameter (m) of the blade respectively

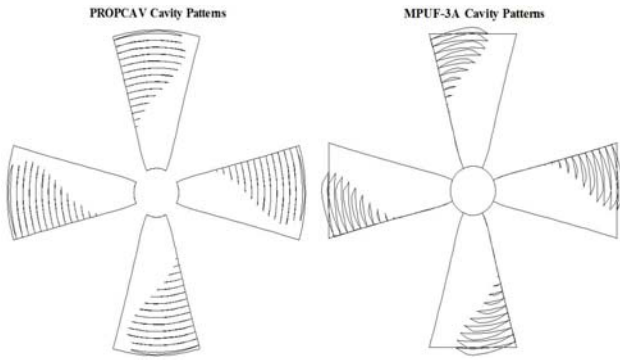


Figure 20: Steady cavity patterns predicted by PROPCAV (left) and by MPUF-3A (right) at $J_s = 0.941$, $RPM = 925$ and $\sigma_n = 5.31$.

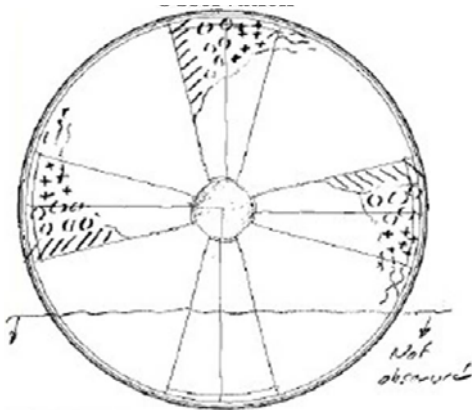


Figure 21: Cavity patterns observed in the experiment at $J_s = 0.941$, $RPM = 925$ and $\sigma_n = 5.31$.

Table 1: Comparison of thrust coefficients K_T

RPM	Experiment K_T	MPUF-3A K_T	PROPCAV K_T
680	0.2433	0.4044	0.4376
760	0.4017	0.4082	0.4510
870	0.3995	0.4185	0.4691
925	0.4602	0.4325	0.4967
960	0.4578	0.4704	0.4989

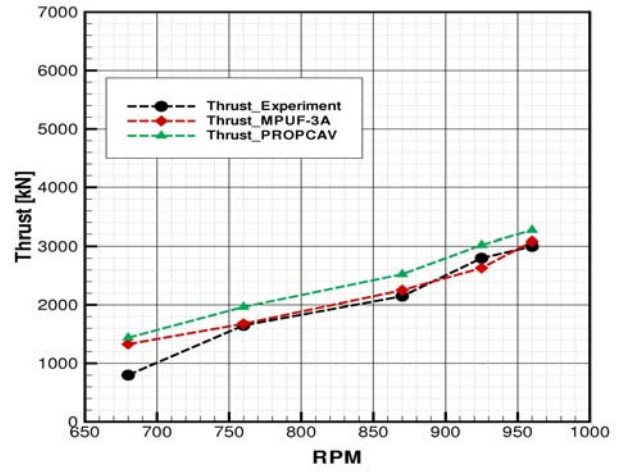


Figure 22: Comparison of the thrust at different RPMs.

CONCLUSIONS AND FUTURE WORK

A coupling scheme which combines a vortex lattice method (MPUF-3A) and a Reynolds-Averaged Navier Stokes solver (FLUENT) has been extended to evaluate the effective wake of a tunnel thruster. The body forces from MPUF-3A are introduced into the momentum equations in FLUENT to represent the time-averaged propeller effect. FLUENT then is used to solve for the velocity field within the entire domain and evaluate the total velocities at the effective wake surface. The effective wake is obtained by subtracting the propeller induced velocity from the total velocity. The new wake is used as an inflow in the next calculation of MPUF-3A to update the body force distributions. This coupling method is solved in an iterative manner until forces are converged.

The performance of the tunnel thruster has been predicted via a vortex lattice method (MPUF-3A) and a boundary element method (PROPCAV). Comparing with experimental measurement, the numerical results from PROPCAV and from MPUF-3A appear to predict the extent of cavitation and thrust reasonably well.

In the future, the tunnel image model in MPUF-3A will be substituted by including the effect of the real tunnel geometry (modeled with panels) to give more accurate evaluation of the propeller performance. The correlations with the experimental data will be used to validate the new tunnel model in MPUF-3A.

ACKNOWLEDGEMENT

Support for this research was provided by the U.S. Office of Naval Research (Contract N00014-07-1-0616) and Phases IV and V of the "Consortium on Cavitation Performance of High Speed Propulsors" with the following current members: American Bureau of Shipping, Daewoo Shipbuilding and Marine Engineering Co. Ltd., Kawasaki Heavy Industry Ltd., Rolls-Royce Marine AB, Rolls-Royce Marine AS, Samsung Heavy Industries Co. Ltd., SSPA AB, Sweden, VA Tech Escher Wyss GmbH, Wärtsilä Propulsion Netherlands B.V.,

Wärtsilä Propulsion Norway AS, Wärtsilä Lips Defense S.A.S., and Wärtsilä CME Zhenjiang Propeller Co. Ltd.

REFERENCES

- Bal, S., Kinnas, S. A., & Lee, H.-S. (2001). 'Numerical Analysis of 2-D and 3-D Cavitating Hydrofoils under a Free Surface'. Journal of Ship Research **45**(1), pp. 34-49.
- Bal, S. & Kinnas, S. A. (2003). 'A Numerical Wave Tank Model for Cavitating Hydrofoils'. Computational Mechanics **32**(4-6), pp. 259-268.
- Choi, J.-K. & Kinnas, S. A. (1998). 'Numerical Water Tunnel in Two and Three Dimensions'. Journal of Ship Research **42**(2), pp. 86-98.
- Choi, J.-K. & Kinnas, S. A. (1999). 'Numerical Model of Cavitating Propeller inside of a Tunnel'. Journal of Fluids Engineering, Transactions of the ASME **121**(2), pp. 297-304.
- Choi, J.-K. & Kinnas, S. A. (2001). 'Prediction of Nonaxisymmetric Effective Wake by a 3-D Euler Solver'. Journal of Ship Research **45**(1), pp. 13-33.
- Ghassemi, H. & Allievi, A. (1999). 'A Computational Method for the Analysis of Fluid Flow and Hydrodynamic Performance of Conventional and Podded Propulsion Systems'. Ocean Engineering International **3**(1), pp. 101-115.
- Kerwin, J., Taylor, T., Black, S. & Mchugh, G. (1997). 'A Coupled Lifting-Surface Analysis Technique or Marine Propellers in Steady Flow'. Proceedings of the Propellers/Shafting Symposium, Society of Naval Architects and Marine Engineers **20**, pp.1-15.
- Kinnas, S. A., Lee, H.-S., & Mueller, A. C. (1998). 'Prediction of Propeller Blade Sheet and Developed Tip Vortex Cavitation'. 22nd Symposium on Naval Hydrodynamics, Washington, D.C., USA.
- Kinnas, S. A., Lee, H.-S., Mishra, B., He, L., Rhee, S.-H. & Balasubramanyam, S. (2006). 'Hydrodynamic Analysis of Podded Propellers'. 11th Propellers/Shafting Symposium, Society of Naval Architects and Marine Engineers, Williamsburg, Virginia, USA.
- Lee, H.-S. & Kinnas, S. A. (2005). 'A BEM for the Modeling of Unsteady Propeller Sheet Cavitation inside of a Cavitation Tunnel'. Computational Mechanics **37**(1), pp. 41-51.
- Sanchez-Caja, A., Rautaheimo, P., & Siikonen, T. (1999). 'Computation of the Incompressible Viscous Flow around a Tractor Thruster Using a Sliding-mesh Technique'. Proceedings of the 7th International Conference on Numerical Ship Hydrodynamics, France.
- Sun, H. & Kinnas, S. A. (2008). 'Performance Prediction of Cavitating Water-jet Propulsors using a Viscous/Inviscid Interactive Method'. Proceedings of 2008 SNAME Annual Meeting and Ship Production Symposium, Houston, Texas, USA.
- Warren, C., Taylor, T., & Kerwin, J. (2000). 'A Coupled Viscous/Potential-Flow Method for the Prediction of Propulsor-Induced Maneuvering Forces'. Proceedings of the Propellers /Shafting Symposium, Society of Naval Architects and Marine Engineers, pp. 20-21.